Absolute crystal and magnetic chiralities in the langasite compound Ba₃NbFe₃Si₂O₁₄ determined by polarized neutron and x-ray scattering

N. Qureshi,[1,*] A. Bombardi,[2] S. Picozzi,[3] P. Barone ●,[3] E. Lelièvre-Berna ●,[1] X. Xu,[4] C. Stock,[5,6] D. F. McMorrow,[7] A. Hearmon ●,[8] F. Fabrizi,[8] P. G. Radaelli,[8] S.-W. Cheong,[4] and L. C. Chapon[1,2]

[1]*Institut Laue-Langevin, 71 avenue des Martyrs, CS 20156, 38042 Grenoble Cedex 9, France*
[2]*Diamond Light Source, Chilton, Didcot, Oxfordshire OX11 0QX, United Kingdom*
[3]*Consiglio Nazionale Delle Ricerche, Istituto SPIN, UOS l'Aquila, Sede di Lavoro CNR-SPIN c/o Universitá G. d'Annunzio, 66100 Chieti, Italy*
[4]*Rutgers Center for Emergent Materials and Department of Physics and Astronomy, Rutgers University, Piscataway, New Jersey 08854, USA*
[5]*Centre for Science at Extreme Conditions, University of Edinburgh, Edinburgh EH9 3FD, United Kingdom*
[6]*School of Physics and Astronomy, University of Edinburgh, Edinburgh EH9 3FD, United Kingdom*
[7]*London Centre for Nanotechnology and Department of Physics and Astronomy, University College London (UCL), Gower Street, London WC1E 6BT, United Kingdom*
[8]*Clarendon Laboratory, Parks Road, Oxford OX1 3PU, United Kingdom*

We present a combined polarized neutron and x-ray scattering study on two enantiopure langasite single crystals aimed at the determination of their absolute structural and magnetic chiralities and the coupling between them. Our respective data sets unambiguously reveal two samples of opposite structural chirality, where the magnetic handedness is pinned by the structural one. Simple energy considerations of the magnetic exchange and single-ion anisotropy parameters reveal that it is not the Dzyaloshinskii-Moriya interaction but the local single-ion anisotropy on a triangular plaquette which plays a key role in stabilizing one of the two magnetic helices.

I. INTRODUCTION

In the last few years, magnetic chirality has been at the heart of various physical phenomena that have attracted considerable attention in condensed matter physics: Skyrmions, or *magnetic bubbles* develop as multi-**q** magnetic structures under an applied magnetic field in chiral crystals such as MnSi or in thin films where inversion symmetry breaking is created at the vacuum interface. Skyrmions possess a topological charge that can be manipulated by spin-polarized currents as recently demonstrated [1]. Under certain conditions magnetic spirals emerging in compounds crystallizing in so-called *ferroaxial* groups [2] develop ferroelectricity and truly magnetically chiral domains can be manipulated by electric fields [3] through a complex trilinear coupling mechanism. Recently, electromagnons have been observed using THz spectroscopy [4] in a pure enantiomer crystal of the langasite compound Ba₃NbFe₃Si₂O₁₄. This compound possesses a chiral crystal structure (space group $P321$) and develops a spiral magnetic ordering below $T_N = 27$ K. Inelastic neutron scattering experiments have revealed directional anisotropy in the spin-wave intensity upon applying a time-reversal symmetry breaking magnetic field along the c axis [5].

In all of these systems there is a direct interplay between the structural and the magnetic chiralities, i.e., the absence of inversion symmetry leads to a magnetic Hamiltonian containing antisymmetric terms (Dzyaloshinskii-Moriya; DM) that favor a given *magnetic handedness*. Determining with a single scattering technique the absolute structural and magnetic chiralities of a crystal is complex. With x rays, determining the structural chirality is a standard task with laboratory equipment done by collecting a large number of Bragg reflections and including the anomalous form factor in the analysis. However, the determination of the absolute magnetic chirality requires the brightness of synchrotron radiation to measure the intrinsically weak magnetic scattering and, at the same time, full control of the absolute polarization of the beam to create a chiral probe [6]. With neutrons, the absolute magnetic chirality is easily determined by employing a polarized beam or measuring the so-called created polarization (by the sample) from an initially unpolarized beam. However, far from the neutron resonances occurring at very high energies, anomalous scattering cannot be used to determine the structural chirality. The only way to probe the structural chirality is to rely on a very weak asymmetry induced by relativistic spin-orbit scattering (also called Schwinger scattering), i.e., a coupling of the neutron spin to the magnetic field generated (in the neutron frame) by the distribution of electric charges in the chiral crystal. The effect of neutron spin–neutron orbit interaction with the atomic Coulomb field was first discussed by J. Schwinger as a method to polarize fast neutrons [7]. It was then experimentally observed in vanadium and CdS single crystals by C. G. Shull [8,9]. Later it was used by Felcher and Peterson to determine the absolute configuration of a CdS single crystal [10].
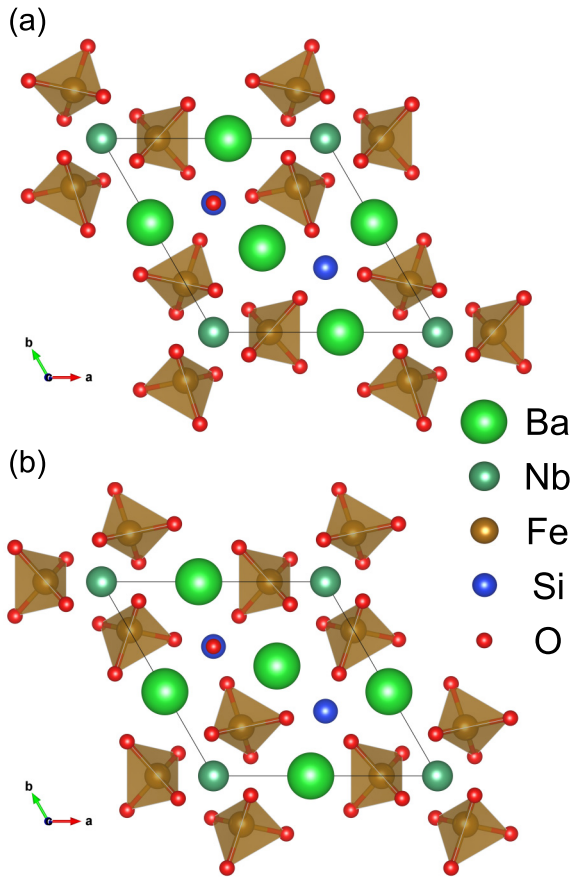
*qureshi@ill.fr

FIG. 1. (a) Left-handed and (b) right-handed crystal structure of $Ba_3NbFe_3Si_2O_{14}$. The atomic positions of the left-handed structure [e.g., Fe atom at (0.249 0 0.5)] are taken from Ref. [11] and have been inverted for the right-handed structure.
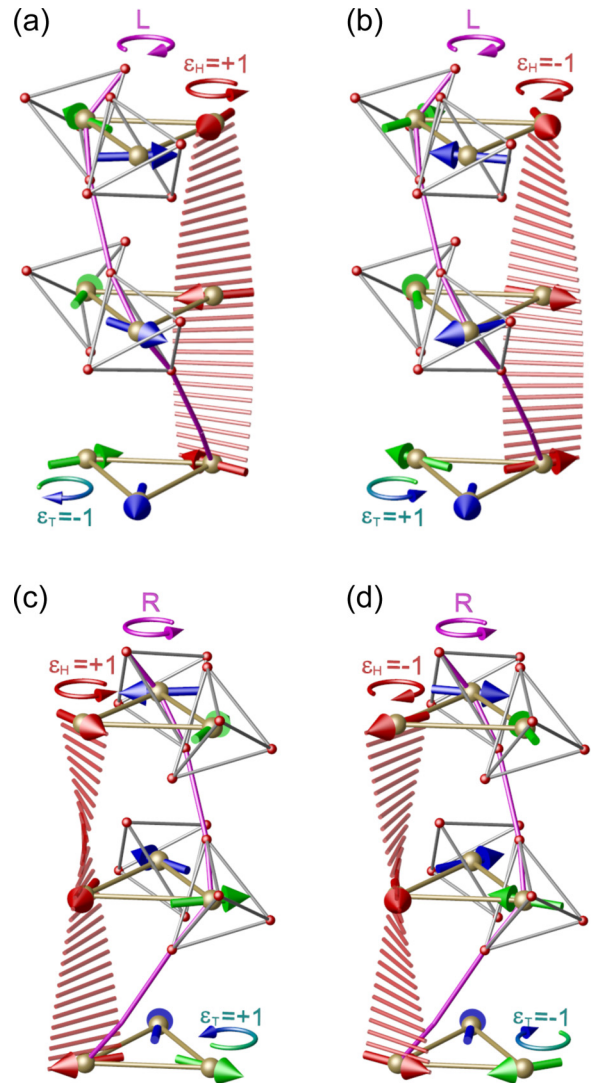

FIG. 2. Four different configurations which all yield the same nuclear and magnetic structure factors. A part of the structure is depicted focusing on a triangular plaquette consisting of three symmetry-equivalent Fe ions at $z = \frac{1}{2}$ which repeat after a translation along c. (a, b) A a left-handed (L) crystal structure which is characterized by the antitrigonometric twist of the Fe-O-O-Fe superexchange pathways (shown in magenta). The helical chirality ϵ_H (rotating cylinders between the spins serve as a guide for the eye) is symbolized by curved arrows on top of the helix. The triangular chirality ϵ_T is symbolized by a clockwise (negative chirality, $\epsilon_T = -1$) or counterclockwise (positive chirality, $\epsilon_T = +1$) arrow positioned between two spins within a triangle. (c, d) The left-handed structural analogs.

In this work, we demonstrate that we can simultaneously determine the structural and magnetic chiralities of langasite single crystals ($Ba_3NbFe_3Si_2O_{14}$) using x rays, on the one hand, and neutrons, on the other hand, employing in each case a single experimental setup and a single specimen without sample cuts or reorientation, and by accessing only a limited number of reflections. We have chosen two single crystals from different batches in order to investigate the coupling of magnetic and structural chiralities. The study shows that our samples reveal a left-handed and a right-handed crystal structure, respectively (according to the definition of Marty *et al.* in Ref. [11]), which is shown in Figs. 1(a) and 1(b) and corresponds to a antitrigonometric or trigonometric twist of the Fe-O-O-Fe superexchange pathway around the c axis illustrated in Fig. 2 by magenta bonds. For each crystal enantiomer there are two possible magnetic states undistinguishable by unpolarized neutron diffraction. For the right-handed structure the first magnetic state is characterized by a positive triangular chirality [12] ($\epsilon_T = +1$), referring to the sense of rotation of the spins within a triangular plaquette when traversed in a counterclockwise fashion, and a right-handed magnetic helicity ($\epsilon_H = +1$), referring to the propagation of the spin structure along the c axis [expressed by the propagation vector $\mathbf{q} = (0\ 0\ 0.14)$]. The other state is characterized by opposite $\epsilon_T = -1$ and $\epsilon_H = -1$. Our

x-ray and neutron results allow us to unambiguously associate the right-handed structural enantiomer with the ($\epsilon_T = +1$, $\epsilon_H = +1$) magnetic state [Fig. 2(c)], which by symmetry argument links a left-handed crystal to the ($\epsilon_T = +1$, $\epsilon_H = -1$) state [Fig. 2(b)]. Our experiments also provide quantitative information about the ellipticity of the magnetic helical modulation, i.e., the envelope of the modulated amplitude in the hexagonal plane. We demonstrate by simple energy considerations of the symmetry-allowed magnetic exchange

and single-ion terms that single-ion anisotropy plays a key role in selecting the chiral ground state.

II. EXPERIMENTAL PROCEDURE

A. Neutron scattering

A small, irregularly shaped single-crystal specimen of $Ba_3NbFe_3Si_2O_{14}$ approximately $4 \times 3 \times 1$ mm^3 in size, grown by the floating-zone technique, was used for the polarized neutron scattering experiment. Enantiopure samples with opposite structural chiralities compared to the one mentioned in Sec. II B were achieved by using different single-crystalline seeds from previous growths. The experiment was carried out at the spin-polarized hot neutron diffractometer D3, where a monochromatic and polarized neutron beam of wavelength $\lambda = 0.825$ Å was selected by the (111) reflection of a Cu_2MnAl Heusler monochromator. A CRYOgenic Polarization Analysis Device [13] (CRYOPAD) was used to create a zero-magnetic-field environment around the sample position in order to suppress the conventional nuclear-magnetic interference scattering. The sample was mounted in a Cryocradle [14], a cryostat containing a fully nonmagnetic Eulerian cradle, which allows *in situ* changes of the sample scattering plane. Guide fields of about 150 G prevent polarization losses along the beam path before and after the CRYOPAD. In the first part of the experiment, which consisted of the absolute crystal structure determination via the neutron spin-orbit scattering, no polarization analysis was carried out and flipping ratios were measured on nuclear Bragg peaks by flipping the polarization of the incoming beam. For the determination of the magnetic handedness a ^{3}He neutron spin filter was used which is hosted by Decpol, a compact detector shielding providing the homogeneous holding field required for the long relaxation time of the ^{3}He polarization. Complete polarization matrices were collected on different magnetic Bragg peaks. Spherical polarization analysis (see Ref. [15] for a detailed description of the technique) adds supplementary selection rules to the general law in magnetic neutron scattering that only spin components perpendicular to the scattering vector can be detected. Nuclear scattering is always a non-spin-flip process. Magnetic components parallel to the incident neutron polarization P_i contribute to the non-spin-flip channels as well, while magnetic scattering from spin components perpendicular to P_i are always spin-flip. Due to the different periodicity of the nuclear and magnetic structures in $Ba_3NbFeSi_2O_{14}$ we can exclude interference terms between nuclear and magnetic scattering. We use the usual reference scheme in polarized neutron scattering where the x direction is defined to be parallel to the scattering vector Q in the horizontal scattering plane, z is the vertical axis of the diffractometer, and y completes the right-handed system. The nine measurements with different incident and final polarization directions can be summarized in the polarization matrix containing the elements $P_{f,i}$. The *chiral terms*, P_{xy} and P_{xz}, indicating the neutron polarization $P_f = P_x$ which has been created along the scattering vector after the scattering of neutrons with $P_i = P_y$ or P_z, reveal direct information about the magnetic handedness.

B. X-ray scattering

A natural surface of the second single crystal of approximately $8 \times 3 \times 1$ mm^3 was used for the x-ray scattering experiment. A small part of the sample was investigated on a laboratory x-ray diffractometer, revealing no signs of inversion or merohedral twinning evidenced by a good refinement to the observed intensities. The magnetic scattering experiment was conducted on the I16 beamline of the Diamond Light Source, in reflection mode. A horizontally polarized beam with a flux of $\approx 10^{13}$ photons per second and a beam size at the sample close to 180×20 μm^2 was delivered by a linear undulator and tuned either at 5.0 keV, to maximize the scattering volume and minimize the noise due to the edges of all the chemical elements present in $Ba_3NbFe_3Si_2O_{14}$, or close to the Fe K edge in resonant condition to determine the structural chirality of the sample through an enhancement of the anomalous scattering. When required, circular polarization of the beam was achieved by transmission through a 100-μm-thick diamond phase plate, reducing the incident flux by 40%. The diamond crystal was aligned close to the (111) reflection in the Laue scattering geometry. For a precise deviation of $\Delta\theta$ from the Bragg condition, the crystal behaves as a quarter-wave plate producing circular light. Due to difficulty in determining the half-wave condition precisely the polarization rate of the beam was close to 80%. Small variations of this value could have occurred during the experiment due to the extreme sensitivity of the polarization to the phase-plate angle. The handedness of the light is determined by the sign of $\Delta\theta$, which was calculated by dynamical scattering theory and confirmed through experimental calibration of the beamline by measuring the x-ray dichroism of a standard ferromagnet. The results on the standard were compared with the ones obtained on the B16 instrument (Diamond Light Source), where the absolute circular polarization of the photon beam was obtained by measuring the natural emission of the bending magnet source above and below the synchrotron orbit plane to get an absolute calibration of the I16 phase-plate setup. The Poincaré-Stokes parameters (P_1, P_2, P_3) describing the photon beam polarizations [left (L_x) and right (R_x) circular polarization] were determined using a procedure explained in Ref. [16].

The specular direction of this crystal was $[\bar{1}\ \bar{2}\ 2]$ and the azimuthal angles are reported with respect to a reference chosen along the $[\bar{1}\ 1\ 0]$ reciprocal direction. The experiment consisted in bringing (in turn) a set of magnetic reflections in Bragg condition. After conventional alignment procedures for each of these peaks, the azimuthal angle was positioned at a value that maximizes the magnetic diffraction intensity. With the sample geometry fixed, and for each polarization state of the photon beam (L_X and R_X), the scattered intensity in a point detector positioned after a linear polarization analyzer is recorded as a function of the deviation angle (η) of this analyzer with respect to the scattering plane. The (004) reflection of a pyrolitic graphite crystal was used for analysis (Bragg angle of $47.6°$, providing a very small miscut). The experimental conditions are exactly as described in the Supplemental Material to Ref. [16].

III. THEORY AND CONVENTIONS

A. Plane-wave convention and direction of Fourier transforms

In order to determine absolute crystal and magnetic configurations the following conventions have been used: A

plane-wave function follows what is usually employed in quantum mechanics and is written as $\exp(ikr - \omega t)$. We also choose to define the scattering vector as the momentum ($\mathbf{Q}$) transferred from the sample to the neutron or photon, therefore $\mathbf{Q} = \mathbf{k}_f - \mathbf{k}_i$ (where $\mathbf{k}_f$ and $\mathbf{k}_i$ refer to the final and incident wave vectors, respectively), a convention usually employed in crystallography and used for the control software of the neutron and x-ray diffractometers used in this study.

With this convention, a forward Fourier transform of a complex function $f(\mathbf{r})$ is written:

$$f(\mathbf{Q}) = \int f(\mathbf{r})e^{-i\mathbf{Q}\cdot\mathbf{r}}d\mathbf{r}. \tag{1}$$

This is known as the *alternative* crystallographic convention [17], which implies that the imaginary part of the scattering amplitudes (b'' for neutron nuclear scattering and f'' for x-ray charge scattering) is written with a negative sign.

B. Description of magnetic structures

For a magnetic structure described by a single wave vector $\mathbf{q}$, the magnetic moment of site j ($\mathbf{m}_j$), in the unit cell L (position vector $\mathbf{R}_L$), can be written

$$\boldsymbol{m}_j(\mathbf{R}_L) = \mathbf{S}_j \exp(i\mathbf{q}\mathbf{R}_L) + \mathbf{S}_j^* \exp(-i\mathbf{q}\mathbf{R}_L), \tag{2}$$

where $\mathbf{S}_j$ is a complex vector and the asterisk denotes complex conjugation. With this convention, a right-handed magnetic helix of unit length (counterclockwise rotation of the moment when propagating along z) is described by the Fourier vector:

$$\mathbf{S}_q = \frac{1}{2}\begin{pmatrix} 1 \\ -i \\ 0 \end{pmatrix}. \tag{3}$$

The opposite magnetic helicity is simply obtained by changing the sign of the imaginary component of this vector.

C. Scattering amplitudes

Magnetic scattering will occur at reciprocal space positions indexed by $\mathbf{Q} = \mathbf{H} \pm \mathbf{q}$, where $\mathbf{H} = (hkl)$. Neglecting the orbital magnetization, the scattered intensity will directly depend, bar the various geometrical factors for x-ray and neutron scattering, on the unit-cell magnetic structure factor:

$$\mathbf{M}(\mathbf{H} + \mathbf{q}) = \sum_j S_j f_j(\mathbf{Q}) \exp(-i\mathbf{Q}\mathbf{r}_j),$$

$$\mathbf{M}(\mathbf{H} - \mathbf{q}) = \sum_j S_j^* f_j(\mathbf{Q}) \exp(-i\mathbf{Q}\mathbf{r}_j).$$

$f_j(\mathbf{Q})$ is the magnetic form factor of ion j, i.e., the Fourier transform of the spin spatial distribution function.

D. Neutron scattering

In the Born approximation, where the scattering amplitude $V(\mathbf{Q})$ is the Fourier transform of the potential function, $V(\mathbf{r})$, the aforementioned conventions require a negative sign in the phase:

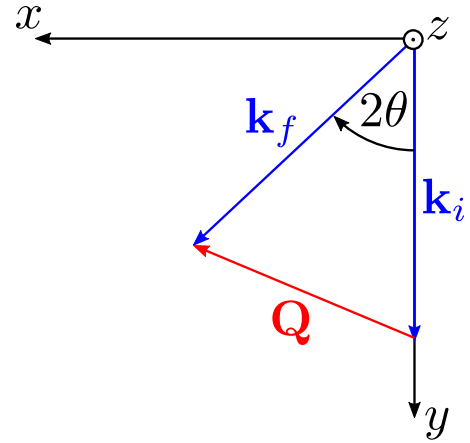$$V(\mathbf{Q}) = -\int V(\mathbf{r})\exp[(-i\mathbf{Q}\mathbf{r})]d\mathbf{r}. \tag{4}$$

FIG. 3. Definition of the momentum transfer for the formalism presented here. We define the scattering angle in the horizontal plane to be positive for scattering to the right of the incoming beam when viewed from the top.

We take the scattering angle 2θ as defined in Fig. 3. Following these conventions the unit cell nuclear scattering amplitude is

$$V_N(\mathbf{Q}) = -\sum_j b_j T_j \exp(-i\mathbf{Q}\mathbf{r}_j), \tag{5}$$

where the sum runs over the atoms j at position $\mathbf{r}_j$ in the primitive crystallographic cell, with b being the scattering length and T the Debye-Waller factor.

The magnetic scattering amplitude is

$$V_M(\mathbf{Q}) = -\gamma r_0 \hat{\boldsymbol{\sigma}} \cdot \mathbf{M}_\perp(\mathbf{Q}), \tag{6}$$

with $\mathbf{M}_\perp(\mathbf{Q})$ the magnetic interaction vector

$$\mathbf{M}_\perp(\mathbf{Q}) = \hat{\mathbf{Q}} \times \mathbf{M}(\mathbf{Q}) \times \hat{\mathbf{Q}} \tag{7}$$

and $\mathbf{M}(\mathbf{Q})$ the magnetic structure factor

$$\mathbf{M}(\mathbf{Q}) = -\sum_j \mathbf{S}_j f_j(\mathbf{Q}) T_j \exp(-i\mathbf{Q}\mathbf{r}_j). \tag{8}$$

In the reference frame of the neutron, the magnetic field generated by a Lorentz transformation of the crystal electric field couples to the neutron spin, leading to the *spin-orbit* (SO) scattering amplitude,

$$V_{\mathrm{SO}}(\mathbf{Q}) = i\frac{\gamma r_0}{2} \cdot \frac{m_e}{m_p} \cdot F_E(\mathbf{Q})\cot(\theta) \cdot \hat{\boldsymbol{\sigma}} \cdot \mathbf{z}, \tag{9}$$

where $\gamma = -1.913$ is the neutron gyromagnetic ratio, r_0 is the classical electron radius, m_e and m_p are the electron and proton masses, $\hat{\boldsymbol{\sigma}}$ is the neutron spin operator, and $F_E(\mathbf{Q})$ is the electrostatic unit-cell structure factor given by

$$F_E(\mathbf{Q}) = -\sum_j [Z_j - f_j(\mathbf{Q})]T_j \exp(-i\mathbf{Q}\mathbf{r}_j)), \tag{10}$$

where Z_j is the atomic number of site j, and $f_j(\mathbf{Q})$ the x-ray atomic form factor for this ion. By polarizing the incident neutron beam along the vertical axis (or, rather, parallel to $\mathbf{k}_i \times \mathbf{k}_f$), one can directly probe the interference between the nuclear and the spin-orbit scattering amplitudes in Bragg condition for a noncentrosymmetric crystal. The ratio of scattered intensities (the so-called flipping ratio R) collected with a

neutron beam polarized parallel and antiparallel to the z axis is given by

$$R = \frac{V_N^2 + V_{SO}^2 + \mathcal{I}}{V_N^2 + V_{SO}^2 - \mathcal{I}}, \tag{11}$$

where $\mathcal{I}$ is the interference

$$\mathcal{I} = p(V_N \cdot V_{SO}^* + V_N^* \cdot V_{SO}) = 2p\Re(V_N \cdot V_{SO}^*) \tag{12}$$

and p is the polarization of the incident neutron beam. The formalism was validated against a certified left-handed quartz sample (see the Appendix).

E. X-ray scattering

With the usual convention of defining the polarization channels perpendicular (σ) and parallel (π) to the scattering plane, the definition of the density matrix of a polarized photon beam, using the Poincaré-Stokes parameters, is given by

$$\boldsymbol{\rho} = \frac{1}{2}\begin{pmatrix} 1 + P_1 & P_2 - iP_3 \\ P_2 + iP_3 & 1 - P_1 \end{pmatrix}. \tag{13}$$

The nonresonant magnetic scattering amplitude V_{NRX} (spin-only contribution) is proportional to $\mathbf{M}(\mathbf{Q}) \cdot \mathbf{B}$, where

$$\mathbf{B} = \begin{pmatrix} \hat{\mathbf{k}}_i \times \hat{\mathbf{k}}_f & -\hat{\mathbf{k}}_f(1 - \hat{\mathbf{k}}_i \cdot \hat{\mathbf{k}}_f) \\ -\hat{\mathbf{k}}_i(1 - \hat{\mathbf{k}}_i \cdot \hat{\mathbf{k}}_f) & \hat{\mathbf{k}}_i \times \hat{\mathbf{k}}_f \end{pmatrix}. \tag{14}$$

The scattered magnetic intensity $I(\eta)$, where η is the polarization analyzer angle, will be proportional to

$$I(\eta) \propto \mathrm{tr}[\mathbf{D}(\eta)\mathbf{V}_{NRX}\boldsymbol{\rho}\mathbf{V}_{NRX}^\dagger], \tag{15}$$

where $\mathbf{D}$ represents the matrix of the analyzer in this basis and is given by

$$\mathbf{D} = \begin{pmatrix} \cos^2(\eta) + \sin^2(\eta)\zeta & \sin(\eta)\cos(\eta)(\zeta - 1) \\ \sin(\eta)\cos(\eta)(\zeta - 1) & \sin^2(\eta) + \cos^2(\eta)\zeta \end{pmatrix}, \tag{16}$$

where $\zeta = \cos^2(2\theta_M)$, with θ_M being the monochromator takeoff angle.

IV. RESULTS AND DISCUSSION

A. Neutron scattering

In order to unambiguously derive the handedness of the crystal and magnetic structure the correct indexing of the nuclear reflections is a crucial starting point. In this particular case the indexation of the first measured Bragg peak is not arbitrary in terms of the sign of the Miller indices, as the flipping ratios due to Schwinger scattering are opposite for Friedel pairs while the nuclear structure factors are of course equal. The correct indexation was verified by comparing the intensities of the (303) and (30$\bar{3}$) nuclear Bragg reflections, the first being half as strong as the {330} reflections and the latter being very weak (see Fig. 4).

1. Schwinger scattering

Appropriate reflections for the experimental detection of Schwinger scattering are those which have a strong nuclear structure factor and an asymmetric flipping ratio significantly
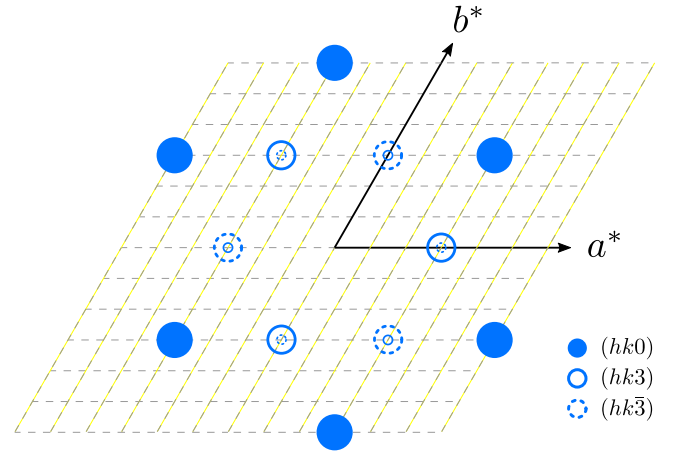

FIG. 4. Sketch of the reciprocal space showing nuclear Bragg reflections {330}, {303}, and {033}. The observed intensities are proportional to the size of the symbols.

different from 1. We have measured 13 of such reflections at $T = 3$ K and the observed flipping ratios were compared to those calculated for a left-handed and a right-handed sample using Eq. (11). The experimental data are in excellent agreement with the predicted flipping ratios of a right-handed sample (see Table I and Fig. 5), which therefore unambiguously determines the absolute crystal configuration (note that if $R < 1$ for a right-handed sample, it is $R > 1$ for a left-handed sample, and vice versa). Quantitative information can be obtained by refining the populations of the two respective inversion twins which reveals a relative volume of 0.985(6) of the right-handed sample, being indeed close to enantiopure. Since all possible twins contribute to the same respective Bragg reflection we are able to address the insidious merohedral twinning which is possible in the trigonal space group $P321$. According to Table I of Chandra et al. [18] the merohedral twinning for space group $P321$ can be expressed as $(\bar{h}\bar{k}l)$ [or, equivalently, $(\bar{k}\bar{h}\bar{l})$] as possible twin operators. It can be shown that the Schwinger flipping ratios R are $R(\bar{h}\bar{k}l) = R(\bar{k}\bar{h}\bar{l}) = R(\bar{h}\bar{k}\bar{l}) = 1 - R(hkl)$ for those reflections measured in this study.

TABLE I. Flipping ratios of selected Bragg reflections. The calculated values correspond to a right-handed crystal structure based on the atomic positions taken from Ref. [11].

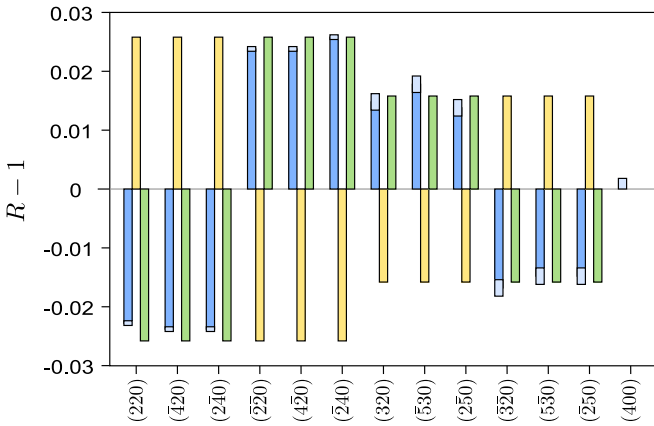| (hkl)	R_{obs}	R_{cal}
(220)	0.977(1)	0.975
$(\bar{4}20)$	0.976(1)	0.975
$(2\bar{4}0)$	0.976(1)	0.975
$(\bar{2}\bar{2}0)$	1.024(1)	1.025
$(4\bar{2}0)$	1.024(1)	1.025
$(\bar{2}40)$	1.026(1)	1.025
(320)	1.015(3)	1.015
$(\bar{5}30)$	1.018(3)	1.015
$(2\bar{5}0)$	1.014(3)	1.015
$(\bar{3}\bar{2}0)$	0.983(3)	0.985
$(5\bar{3}0)$	0.985(3)	0.985
$(\bar{2}50)$	0.985(3)	0.985
(400)	1.001(2)	1

FIG. 5. Bar chart of the observed flipping ratios ($R - 1$) shown in the left bar of each (hkl) reflection [blue; lighter area represents $(R - 1) \pm \sigma$] compared to the calculated values for a left-handed structure (middle bar of each (*hkl*) reflection; yellow) and a right-handed structure (right bar of each (*hkl*) reflection; green).

Therefore, if we refine the relative twin volume to 0.985(6) for the right-handed structure, we have a volume of 1-0.985(6), which can be attributed to the left-handed structure or merohedral twins of the right-handed structure, which shows that our neutron results are not affected by the additional structure complexity. To finally corroborate the validity and robustness of our results we have used the structure model proposed in Ref. [19] to calculate the Schwinger flipping ratios. As a matter of fact the calculated values only differ in the fourth decimal digit, while our measured flipping ratios have an uncertainty of at least 0.001. This ultimately shows that subtle differences in the structural parameters do not influence the asymmetry of the flipping ratios in a significant way. Figure 6 shows a sketch of the results in reciprocal space for the (220) and (320) reflections and their crystallographic equivalents, which reflects the threefold rotation symmetry but an absence of inversion symmetry, i.e., the flipping ratios of Friedel pairs are inverted.

2. Magnetic scattering

In order to derive the helical chirality full polarization matrices were recorded at $T = 3\,$K by analyzing the spin of the scattered neutrons in dependence of their incident spin. The handedness of the triangular chirality can be derived from the integrated intensities of the magnetic Bragg peaks. The fact that the (1 0 0.14) reflection is strong, while the intensity of the (1 0 −0.14) reflection is almost 0 is consistent with four different magnetic structures, where triangular and helical chirality have opposite signs for a left-handed crystal structure and the same signs for a right-handed crystal structure (see Fig. 2). Using the information acquired from the Schwinger scattering experiments described in the section above we can therefore narrow the choice of possible magnetic structures to the ones depicted in Fig. 2(c) and Fig. 2(d), which we denote R(1,1) and R(−1, −1), respectively, for a right-handed crystal structure with the given chiralities (ϵ_T, ϵ_H). The last necessary piece of information therefore lies in the sign of the polarization matrix elements P_{xy} and P_{xz}, which are directly related to the helical handedness. We have recorded the polarization matrices of five different magnetic Bragg peaks and compared the observed chiral terms P_{xy} and P_{xz} to the calculated values derived from the magnetic models for a right-handed sample. The data shown here have been normalized to the time-dependent ^{3}He spin-filter efficiency, which was periodically monitored by measuring the P_{zz} term of a nuclear reflection, and an initial neutron polarization of $p_0 = 0.935$ was taken into account for the calculations [20]. Each magnetic moment within a triangular plaquette lies on a twofold axis which goes through the center of the triangle (2 ∥ *a*, *b*, [110]). In order to account for an eventual site anisotropy we have defined the real part of the Fourier components of the magnetic moments to lie along this twofold axis, while the imaginary part is perpendicular to it. Neutron polarimetry is not sensitive to the size of the magnetic moments when nuclear-magnetic interference is absent, for which we have fixed the imaginary part, i.e., the only refined parameter was the real part of the Fourier component. The refinement has been carried out using the MAG2POL program [21]. All
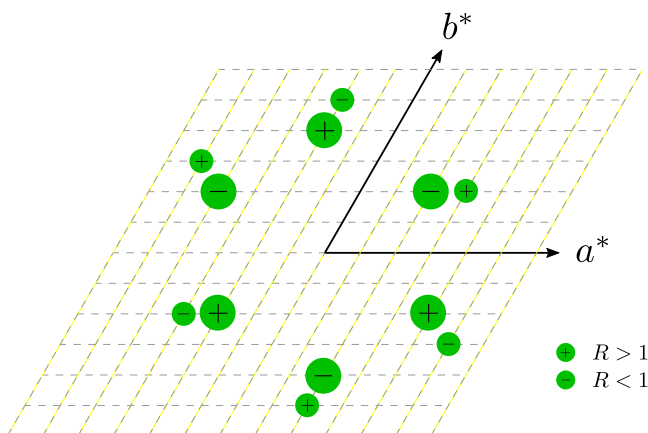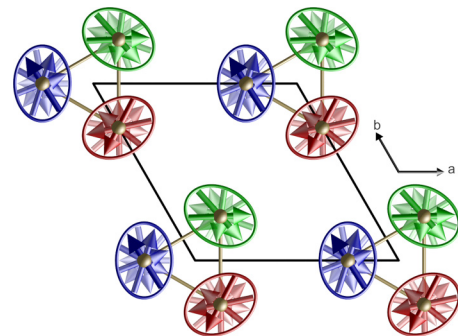

FIG. 6. Sketch of the reciprocal space showing the flipping ratios R of selected Bragg reflections. The observed asymmetries are proportional to the size of the symbols.

FIG. 7. Visualization of the resulting magnetic structure from the refinement to the polarimetry data. The envelope of the spin modulation along the *c* axis (decreasing transparency corresponds to an increasing *c* component) is elliptical, with the main axis perpendicular to the twofold rotation axis being larger then the one along it. This results in a site anisotropy expressed by $S^h/S^e = 0.91(3)$, which has been exaggerated by a factor of 3 for visibility.

TABLE II. Observed polarization matrix entries P_{xy} and P_{xz} and the calculated ones corresponding to the two models R(1,1) and R($-1, -1$) shown in Fig. 2(c) and Fig. 2(d), respectively.

(hkl)	P_{xy}			P_{xz}		
	Observed	R(1,1)	R($-1, -1$)	Observed	R(1,1)	R($-1, -1$)
$(\bar{1}\,0\,0) - \mathbf{q}$	$-0.336(7)$	-0.363	0.363	$-0.369(7)$	-0.363	0.363
$(\bar{1}\,1\,1) + \mathbf{q}$	$-0.951(7)$	-0.949	0.949	$-0.949(6)$	-0.949	0.949
$(0\,\bar{1}\,1) + \mathbf{q}$	$-0.946(4)$	-0.945	0.945	$-0.952(4)$	-0.945	0.945
$(\bar{1}\,0\,1) - \mathbf{q}$	$0.950(4)$	0.941	-0.941	$0.950(4)$	0.941	-0.941
$(0\,1\,1) - \mathbf{q}$	$0.940(4)$	0.937	-0.937	$0.944(4)$	0.937	-0.937

observed polarization matrices can nicely be explained with an elliptical envelope of the magnetic moments which is elongated along the direction perpendicular to the respective twofold axis, yielding an ellipticity of $S^h/S^e = 0.91(3)$ ($\chi^2 = 26.8$), where S^h and S^e are the hard and easy magnetic axes, respectively (Fig. 7). The results concerning the chiral terms are listed in Table II and the signs of the matrix entries clearly state that the investigated sample has a positive helical chirality, which therefore follows the handedness of the right-handed crystal structure. The comparison between calculated and observed polarization matrices is shown in Fig. 8.

B. X-ray scattering

1. Anomalous scattering

An x-ray diffraction experiment with a linearly polarized incident beam is sensitive to the chirality of the investigated sample only through the interference of the anomalous part of the atomic form factor. These terms are usually small unless the measurement is performed in the vicinity of the absorption edge of one of the elements present in the material. This technique, first used by Bijovet, is now routinely used to determine the chirality in complex organic samples. Our approach is an extreme version of the MAD technique as, once the convention in use on I16 is established, i.e., right handed-ness of the diffractometer and $\mathbf{Q} = \mathbf{k}_f - \mathbf{k}_i$ convention, the behavior of the reflection through the Fe K absorption edge immediately returns information about the sample chirality. It is important to mention that it is necessary to distinguish the

Friedel pairs as their behavior through the absorption edge is reversed.

The expected anomalous behavior through the Fe absorption K edge was simulated from the accepted crystallographic data files for various reflections. The simulations suggested that large differences would occur for some reflections, showing an intensity increase for the right-handed crystal through the transition, whereas the left-handed counterpart would decrease through the transition. Other reflections would show no contrast at all. A further advantage of this approach is that it allows us to explore the sample's structural chirality under the same experimental conditions that were used to probe the magnetic properties of the sample with circularly polarized light, making possible a self-consistent investigation. Figure 9 shows the intensity measured at room temperature as a function of the energy for four different reflections together with the simulations obtained for the left-handed ($x_{Fe1}=0.249$) and right-handed ($x_{Fe1}=0.751$) crystal. All the curves have been renormalized to their maximum value and the upper x scale for
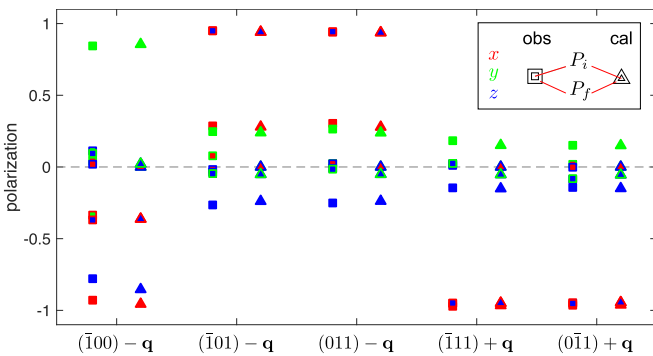

FIG. 8. Observed (squares) and calculated (triangles) polarization values P_{if} for incident neutrons polarized along P_i (inner symbol color) and polarization analysis along P_f (symbol edge color) for the three directions x (red symbols), y (green symbols), and z (blue symbols).
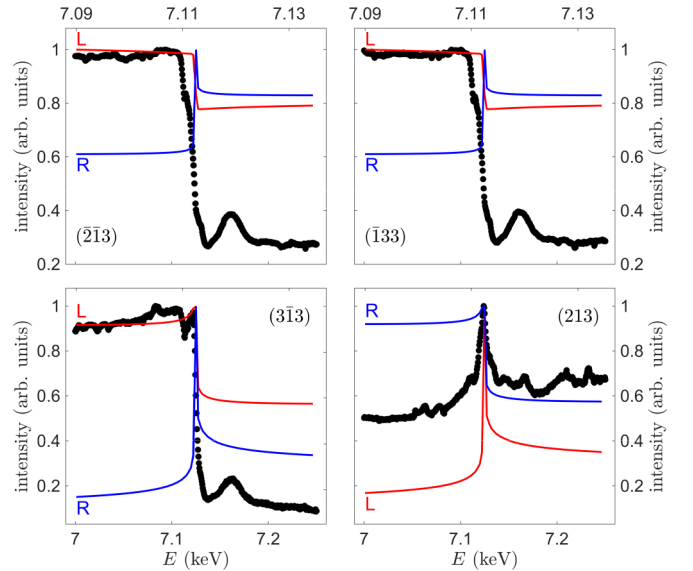

FIG. 9. The behavior of four noncoplanar reflections shows great contrast in the simulations for the left-handed (red lines) and right-handed (blue lines) enantiomers. Black circles represent the renormalized experimental intensity of the four reflections measured in the center of our specimen at room temperature. As is immediately evident, only simulations with the left-handed structure match the trend of the experimental data. No attempt was made to simulate the subtle feature shown by the experimental data across the transition.
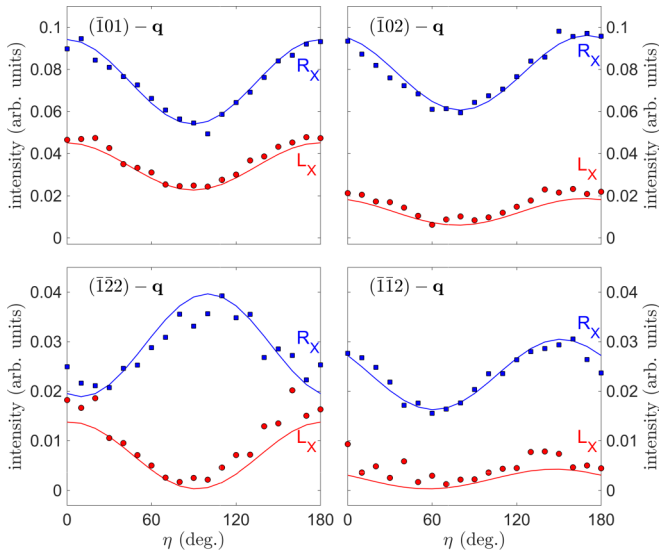
FIG. 10. The x-ray dichroic intensity as a function of the deviation angle η of the linear polarization analyzer from the scattering plane for four different magnetic Bragg reflections at $T = 5$ K. Red circles represent data taken with a photon beam of left-handed polarization; blue squares, data measured with a photon beam of right-handed polarization. The calculated intensities (fitted with a global scale factor) are based on a left-handed enantiomer and are shown as solid lines in the corresponding colors.

the energy refers to the simulations. The difference between the two chiralities is obvious, and in principle even only one reflection can be used to establish the sample behavior provided that the naming convention is correct, which requires the measurement of at least three noncoplanar reflections. Note that the simulations are based solely on the anomalous scattering data available in the CXRO [22] databases, in which the obtainable values are purely atomic and not available next to the edge. Hence, the simulations do not include correlations and/or the detailed form of the material's electronic density of states. The real experiment is sensitive not only to the details of the density of states but also to other phenomena, e.g., diffraction anomalous fine structure, that are not included in the simulations, which explains the quantitative differences between observed and simulated data. However, for the purpose of establishing the structural chirality these additional features are superfluous. Finally, in analogy to Sec. IV A 1 we want to comment on the possible merohedral twinning of the sample. For a significantly twinned sample our simulations reveal that the $(\bar{2}\bar{1}3)$ reflection (upper-left panel in Fig. 9) would present jumps up and down of similar size, which is at odd with our experimental data.

2. Circularly polarized light

The magnetic chirality was investigated at $T = 5$ K using the same single crystal as for the anomalous scattering experiment, which was determined to have a left-handed crystal structure (Sec. IV B 1). A large area of the sample was mapped with respect to its magnetic chirality, revealing the same character, from which we can deduce that it is magnetically enantiopure and, given the relationship between structure and magnetism, also structurally enantiopure. Figure 10 shows the
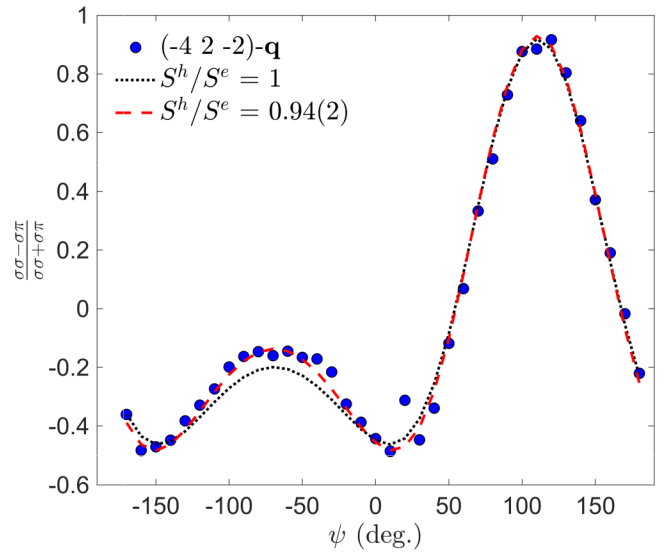

FIG. 11. Azimuthal scan with incident polarization perpendicular to the scattering plane under the nonresonant condition on the $(-4\,2\,-2) - \mathbf{q}$ reflection. The ellipticity is given by the ratio of the spin component along the hard axis (S^h) to that along the easy axis (S^e) of the envelope.

scattered intensity as a function of the deviation angle η of the linear polarization analyzer from the scattering plane for each polarization state of the photon beam (left-handed, red circles; right-handed, blue squares) and for four different magnetic Bragg peaks. The calculated values for the left-handed (red lines) and right-handed (blue lines) beam polarization are based on a left-handed magnetic spiral (note that only one parameter—a global scale factor—was refined). As can be seen, the agreement between the observed and the calculated intensities is excellent and confirms the results from the neutron experiments insofar as the magnetic chirality follows the structural one. Note that for a right-handed magnetic chirality the calculated curves would be inverted between left-handed and right-handed beam polarization.

3. Ellipticity with x rays

In Fig. 11 we show the results of the azimuthal scans performed with incident polarization perpendicular to the scattering plane σ in nonresonant condition on the magnetic reflection $(-4\,2\,-2)$-$\mathbf{q}$, the final polarization was analyzed in the two channels, σ and π. In this configuration XMS is not sensitive to the helicity of the magnetic structure but extremely sensitive to the direction of the magnetic moment and to the different components of the magnetic interaction vector. The reflection's azimuthal dependence can be well matched within a circular helical modulation, however, if the real and imaginary parts of the Fourier components describing the magnetic structure are allowed to be different, a much better agreement is obtained when $S^h/S^e = 0.94(2)$. This value excellently matches our result obtained with the spherical neutron polarimetry method.

C. Spin-orbit coupling effects in langasites

Following our experimental results, which state that for a given crystal chirality a single magnetic chirality is

established, we elucidate the energy balance between exchange and single-ion anisotropy (SIA) terms with the aim of revealing which parameter is responsible for the coupling between both chiralities.

1. Spin-orbit coupling in a single triangle

Assuming that the spin-orbit coupling (SOC) with strength λ acts as a perturbation, i.e., the exchange interaction $J \gg \lambda$, then the ground state for spins $\mathbf{S}_j$ on a single triangle has the standard $120°$ configuration. The total energy can be written as $E = E_0 + E_{\mathrm{DMI}} + E_{\mathrm{SIA}}$, where E_0 is the energy contribution due to symmetric exchange coupling, E_{DMI} is the Dzyaloshinskii-Moriya correction and E_{SIA} is the magnetic single-ion anisotropy. The first SOC-mediated correction only depends on the triangular chirality ϵ_T, since the angle between neighboring spins is always $120°$, hence

$$E_{\mathrm{DMI}} = -\epsilon_T DM \sin\left(\frac{2\pi}{3}\right), \tag{17}$$

where DM is a constant proportional to λ, the bare SOC. The second contribution can be expressed as

$$H_{\mathrm{aniso}} = \frac{M}{3} \sum_{j=a,b,c} \left[(S_j^h)^2 - (S_j^e)^2\right], \tag{18}$$

where M is again a constant ($\propto \lambda^2$) and $S_j^{h(e)}$ are the spin components along the hard (easy) axis on each vertex of the triangle. Since the hard (easy) axis in the langasite structure rotates by $120°$ at each triangle vertex, the SIA contribution can be expressed as

$$E_{\mathrm{SIA}} = \frac{M}{3}[\cos(2\phi) + \cos(2\phi_+) + \cos(2\phi_-)], \tag{19}$$

with $\phi_+ = \phi + (\epsilon_T - 1)\frac{2\pi}{3}$ and $\phi_- = \phi - (\epsilon_T - 1)\frac{2\pi}{3}$. One immediately finds that $E_{\mathrm{SIA}}(\epsilon_T = -1) = 0$ for any value of the spin rotation angle ϕ measured at a particular site. On the other hand, for a positive triangular chirality $\epsilon_T = 1$ one obtains $E_{\mathrm{SIA}}(\epsilon_T = 1) = M \cos(2\phi)$ with minima at $\phi = \pm\pi/2$.

2. Chirality in a triangle chain

The helical incommensurate spin configuration can be explained by a Heisenberg model with symmetric exchange coupling only and emerges from the different nearest-neighbor exchange couplings J_3, J_4, J_5 that reflect the lattice chirality of the langasite structure. [23] Assuming that the relevant physics occur along the c axis (J_4 connects equivalent corners of two triangles separated along c, J_5 corresponds to the twisted Fe-O-O-Fe superexchange pathway shown as magenta bonds in Fig. 2, and J_3 denotes the third possible exchange interaction between two triangles), the Hamiltonian for the chain reads

$$H = \sum_i \left[J_4 \mathbf{S}_i^a \cdot \mathbf{S}_{i+1}^a + J_3 \mathbf{S}_i^a \cdot \mathbf{S}_{i+1}^b + J_5 \mathbf{S}_i^a \cdot \mathbf{S}_{i+1}^c\right], \tag{20}$$

where a, b, c label the different spins on the vertex of each triangles lying on the ith layer along the c axis. When SIA is not included, the energy depends only on the angle α between correspondent spins in neighboring layers and the

energy becomes

$$\frac{1}{N}E(\alpha) = J_4 \cos(\alpha) + J_3 \cos\left(\alpha + \epsilon_T \frac{2\pi}{3}\right)$$
$$+ J_5 \cos\left(\alpha - \epsilon_T \frac{2\pi}{3}\right). \tag{21}$$

The optimal angle α, which also defines the pitch $q_0 = \alpha/2\pi$ of the spin helix, is given by

$$\tan(\alpha) = -\frac{c_2}{c_1}, \tag{22}$$

with

$$2c_1 = (J_3 + J_5) - 2J_4, \quad 2c_2 = \epsilon_T \sqrt{3}(J_5 - J_3). \tag{23}$$

The corresponding energy can be expressed as $E(\alpha) = -N\sqrt{c_1^2 + c_2^2}$, from which one sees that it does not depend on the chirality ϵ_T. On the other hand, Eqs. (22) and (23) define the helix chirality ϵ_H, which depends both on ϵ_T and on the exchange couplings. If we assume that $J_3 = 0.13$ meV, $J_4 = 0.1$ meV, and $J_5 = 0.33$ meV for a left-handed structural chirality (from Ref. [23]), then $\epsilon_T \epsilon_H = -1$ and the ($\epsilon_T = +1$, $\epsilon_H = -1$) and ($\epsilon_T = -1$, $\epsilon_H = +1$) configurations are degenerate. Furthermore, the pitch of the incommensurate helix is found to be $q_0 = 0.148 \sim 1/7$.

3. Dzyaloshinskii-Moriya interaction along the c axis

The helical configuration is therefore allowed by considering the asymmetry between the symmetric exchange interactions, rather than antisymmetric DMI, that appears as a small correction only, with the Hamiltonian

$$H_{\mathrm{DMI}} = \sum_i DM_4 \mathbf{S}_i^a \times \mathbf{S}_{i+1}^a + DM_3 \mathbf{S}_i^a \times \mathbf{S}_{i+1}^b$$
$$+ DM_5 \mathbf{S}_i^a \times \mathbf{S}_{i+1}^c. \tag{24}$$

Since the energy of each layer is not affected by the DMI along the c direction, the inclusion of DMI implies only a slight modification of Eq. (23), namely,

$$2c_1 = (J_3 + J_5) - 2J_4 - \epsilon_T \sqrt{3}(DM_5 - DM_3),$$
$$2c = \epsilon_T \sqrt{3}(J_5 - J_3) - 2DM_4 + DM_5 + DM_3, \tag{25}$$

while Eq. (22) is not changed. Since the DMI is usually a small correction to the exchange terms, these findings also imply that the ordering wave vector is only slightly changed, even if differently for positive or negative ϵ_T. One would also expect the DMI to lift the degeneracy between the ($\epsilon_T = +1$, $\epsilon_H = -1$) and ($\epsilon_T = -1$, $\epsilon_H = +1$) solutions, however, if one assumes $DM_i \sim \frac{\Delta_g}{g} J_i$ [i.e., the DMI correction is equally proportional to the corresponding exchange interaction (see Eq. 2.6 in Ref. [24] or Ref. [25]); g and $\frac{\Delta_g}{g}$ are the gyromagnetic ratio and its deviation from the free-electron value, respectively], it can be shown that the optimal energy is again independent of ϵ_T, therefore the DMI along the c axis is apparently not sufficient to lift the chirality degeneracy. In fact, $E(\alpha) = N\sqrt{\mathcal{E}_0 + \partial\mathcal{E}(\epsilon_T)}$, where

$$\partial\mathcal{E}(\epsilon_T) = \frac{3}{2}[(J_5 - J_3)(DM_5 + DM_3 - 2DM_4)$$
$$- (DM_5 - DM_3)(J_5 + J_3 - 2J_4)], \tag{26}$$

and $\mathcal{E}_0$ is independent of the triangle chirality. One immediately recognizes that $\partial\mathcal{E}(\epsilon_T) = 0$ if $DM_i = gJ_i$.

4. Ellipticity and the role of SIA

When considering the SIA effects, the energy does not depend on the angle α only, i.e., on the angle between spins in neighboring layers, but also on the spin directions expressed by ϕ_i. By including H_{aniso} and H_{DMI} in H one obtains the most interesting finding, which concerns the helix ellipticity measured as the ratio of the averaged spin components along the hard and the easy axis, $\overline{S_i^h}/\overline{S_i^e}$. Without SIA, i.e., for $\epsilon_T = -1$, this ratio is always 1. On the other hand, for a positive triangular chirality the spiral becomes elliptic in order to enhance the energy gain due to SIA even if M is an order of magnitude smaller then J_i. We find $\overline{S_i^h}/\overline{S_i^e} \approx 0.9$ for the assumed values of all coupling constants [26]. This result is rather independent of the SOC strength. The SIA induces an elliptical spiral in the ($\epsilon_T = +1$, $\epsilon_H = +1$) and ($\epsilon_T = +1$, $\epsilon_H = -1$) configurations only, which correspond to right-handed and left-handed crystal structures, respectively. As a consequence, the local magnetic anisotropy is responsible for a qualitative difference between positive and negative helical chiralities.

In summary of the above Secs. IV C 1–IV C 4 we have shown that the absolute chirality $\epsilon_H\epsilon_T$ is dictated by the symmetric exchanges along c, which in turn are fixed by the structural chirality (Sec. IV C 2). However, the DMI between two triangles along the c axis does not allow us to distinguish between the two helical configurations with fixed absolute chirality, as discussed in Sec. IV C 3. On the other hand, the SOC effects introduced in Sec. IV C 1, i.e., the DMI within a single triangle and the SIA, impose a fixed value of ϵ_T, which, on its own, is not experimentally accessible. Nevertheless, only the SIA can explain the onset of an elliptic spiral, as shown in Sec. IV C 4. Both the absolute chirality $\epsilon_H\epsilon_T$ and the ellipticity, which are governed by structural chirality and SIA, respectively, are experimentally accessible using spherical neutron polarimetry and circularly polarized x-ray scattering, allowing us to deduce the driving forces for a particular magnetic configuration.

V. CONCLUSION

We have presented a combination of polarized neutron and x-ray scattering on two enantiopure langasite single crystals of different structural chiralities. Given the complexity of the analysis of absolute chiralities we have carefully validated our neutron and x-ray formalisms and experimental setups by using certified reference samples in order to corroborate our results concerning the structural chiralities. The chiral link between structure and magnetism is independent of the sample and the technique used, since we have carefully derived the neutron and x-ray equations and apply them in the analysis of both the structural and the magnetic data. In the neutron part we have exploited integrated intensities, spherical neutron polarimetry, and Schwinger scattering in order to unambiguously determine the absolute structural, magnetic triangular, and magnetic helical handedness of one and the same sample in the same experiment. The flipping

ratios—arising from the interference between nuclear and spin-orbit scattering—of the measured set of reflections can be calculated very precisely based on the right-handed enantiomorph of the $Ba_3NbFe_3Si_2O_{14}$ structure. Such an enantiomorph can host two different magnetic structures where the triangular and helical handedness are the same within each model but are opposite between the models [see Figs. 2(c) and 2(d)]. Spherical neutron polarimetry, which can differentiate between both models as the helical handedness can directly be accessed via the created polarization along the scattering vector for initial polarization directions perpendicular to it, clearly proved that the helical chirality follows the structural one, which results in the structure model shown in Fig. 2(c). In the x-ray part we have combined anomalous scattering and circular dichroism, which reveal information concerning the nuclear and magnetic chirality, respectively. Our results on a second sample indicate a left-handed enantiomorph, which reveals a left-handed magnetic spiral [see Fig. 2(b)]. Therefore, our data undoubtedly suggest the same handedness for the nuclear structure and for the helical chirality. By comparison with Fig. 2 one may confirm that these two structures reveal a positive triangular chirality, which in principle allows an ellipticity of the spin envelope as shown in Sec. IV C 4. Both our employed techniques prove that the envelope of the spin modulation in the hexagonal plane is indeed significantly elongated along the direction perpendicular to the twofold rotation axis. This result is in perfect agreement with the reported helical bunching [27] stating that the rotation angle between successive spins along the c axis is smaller when the spins are parallel to the easy axis. Following the calculations shown in Sec. IV C the DM interaction alone is not sufficient to lift the degeneracy between the different magnetic models and therefore to impose a helical chirality based on the antisymmetric exchange interactions between two triangles at different c values within the crystal structure (assuming that the DM interactions DM_i are equally proportial to the respective exchange parameters J_i). It would rather seem that in this langasite compound the local anisotropy of a triangular plaquette is the driving force, which dictates the helical handedness in dependence on the exchange couplings J_3, J_4, and J_5. A major role of the exchange interactions over the DM effect in the magnetic properties of $Ba_3NbFe_3Si_2O_{14}$ can also be deduced from the fact that the Néel temperature strongly increases upon application of pressure [28]. This scenario of increasing exchange interactions as a direct consequence of the decrease in the unit-cell volume is in stark contrast to the MnSi compound, where the application of pressure drives the system into a quantum phase transition [29].

TABLE III. Flipping ratios of selected Bragg reflections. The calculated values correspond to a left-handed quartz sample (space group $P3_221$).

(hkl)	R_{obs}	R_{cal}
(110)	1.005(1)	1.009
(2$\bar{1}$0)	0.993(1)	0.991
($\bar{1}$20)	0.996(1)	0.991
($\bar{2}$10)	1.002(1)	1.009
($\bar{1}\bar{1}$0)	0.995(1)	0.991
(1$\bar{2}$0)	1.002(1)	1.009
(201)	1.000(1)	1.000

APPENDIX: QUARTZ SAMPLE

In order to verify our results in Sec. IV and the formalism deduced in Sec. III C an additional polarized neutron experiment on D3 using a certified left-handed quartz sample purchased from Crystran Ltd. [30] has been carried out. The observed nuclear Bragg reflections were indexed in order to have the correct intensity ratio between them as described above for the langasite sample and the structural handedness was investigated by measuring the flipping ratios due to Schwinger scattering. The observed flipping ratios agree well (see Table III) with the calculated ones based on a left-handed quartz structure (space group $P3_221$), which therefore confirms the correctness of the employed formalism including the definition of momentum transfer.

An additional proof of the structural handedness was supplied by performing an experiment using linearly polarized light with a wavelength of 668 nm. The rotation of the plane of polarization is proportional to the sample thickness and is expected to be ∼45° for the used sample (3-mm thickness). The experiment was conducted by placing a polarizer (used as an analyzer) between the sample and the detector and by adjusting its orientation in order to reduce the detected intensity to its minimum. The left-handed quartz sample was then positioned with the c axis along the light beam and the analyzer angle was adjusted to recover the initial (minimum) intensity. The sample rotated the plane of polarization of the light by roughly 40° counterclockwise when viewed from the source along the direction of light propagation, which agrees with the sample having a left-handed crystal structure [31]. The results are in perfect agreement with the polarized neutron data and therefore validate the results presented above.

[1] N. Romming, C. Hanneken, M. Menzel, J. E. Bickel, B. Wolter, K. von Bergmann, A. Kubetzka, and R. Wiesendanger, Science **341**, 636 (2013).

[2] R. D. Johnson, L. C. Chapon, D. D. Khalyavin, P. Manuel, P. G. Radaelli, and C. Martin, Phys. Rev. Lett. **108**, 067201 (2012).

[3] A. J. Hearmon, F. Fabrizi, L. C. Chapon, R. D. Johnson, D. Prabhakaran, S. V. Streltsov, P. J. Brown, and P. G. Radaelli, Phys. Rev. Lett. **108**, 237201 (2012).

[4] L. Chaix, S. de Brion, F. Lévy-Bertrand, V. Simonet, R. Ballou, B. Canals, P. Lejay, J. B. Brubach, G. Creff, F. Willaert *et al.*, Phys. Rev. Lett. **110**, 157208 (2013).

[5] C. Stock, R. D. Johnson, N. Giles-Donovan, M. Songvilay, J. A. Rodriguez-Rivera, N. Lee, X. Xu, P. G. Radaelli, L. C. Chapon, A. Bombardi *et al.*, Phys. Rev. B **100**, 134429 (2019).

[6] F. Fabrizi, H. C. Walker, L. Paolasini, F. de Bergevin, A. T. Boothroyd, D. Prabhakaran, and D. F. McMorrow, Phys. Rev. Lett. **102**, 237205 (2009).

[7] J. Schwinger, Phys. Rev. **73**, 407 (1948).

[8] C. G. Shull, Phys. Rev. Lett. **10**, 297 (1963).

[9] C. G. Shull, Trans. Am. Cryst. Assoc. **3**, 1 (1967).

[10] G. P. Felcher and S. W. Peterson, Acta Crystallogr., Sect. A: Found. Crystallogr. **31**, 76 (1975).

[11] K. Marty, V. Simonet, E. Ressouche, R. Ballou, P. Lejay, and P. Bordet, Phys. Rev. Lett. **101**, 247201 (2008).

[12] It should be mentioned that we adopt the term *triangular chirality* from earlier publications in the field, e.g., Refs. [11] and [23]. However, a flat or two-dimensional object like the triangular plaquette in the langasite structure can in principle not be called chiral due to the definition of chirality, which states that a chiral object cannot be superposed with its mirror by a combination of rotations and translations.

[13] E. Lelièvre-Berna, E. Bourgeat-Lami, P. Fouilloux, B. Geffray, Y. Gibert, K. Kakurai, N. Kernavanois, B. Longuet, F. Mantegezza, M. Nakamura *et al.*, Physica B **356**, 131 (2005).

[14] E. Lelièvre-Berna, in *International Symposium on Optical Science and Technology*, edited by N. J. Halas (SPIE, Bellingham, WA, 2002), p. 112.

[15] P. J. Brown, in *Neutron Scattering from Magnetic Materials*, edited by T. Chatterji (Elsevier, St. Louis, MO, 2006), chap. 5, p. 215.

[16] R. D. Johnson, P. Barone, A. Bombardi, R. J. Bean, S. Picozzi, P. G. Radaelli, Y. S. Oh, S.-W. Cheong, and L. C. Chapon, Phys. Rev. Lett. **110**, 217206 (2013).

[17] U. Shmueli (Ed.), *International Tables for Crystallography, Vol. B: Reciprocal Space* (D. Reidel, Dordrecht, 1993).

[18] N. Chandra, K. R. Acharya, and P. C. E. Moody, Acta Crystallogr., Sect. D: Biol. Crystallogr. **55**, 1750 (1999).

[19] A. P. Dudka, A. M. Balbashov, and I. S. Lyubutin, Cryst. Growth Des. **16**, 4943 (2016).

[20] We want to point out that it is possible to refine the initial neutron polarization together with the magnetic structure parameters for the case where chiral scattering is present. We indeed find the best results for $p_0 = 0.935$, which is the known polarization on D3.

[21] N. Qureshi, J. Appl. Cryst. **52**, 175 (2019).

[22] B. L. Henke, E. M. Gullikson, and J. C. Davis, At. Data Nucl. Data Tables **54**, 181 (1993).

[23] C. Stock, L. C. Chapon, A. Schneidewind, Y. Su, P. G. Radaelli, D. F. McMorrow, A. Bombardi, N. Lee, and S.-W. Cheong, Phys. Rev. B **83**, 104426 (2011).

[24] T. Moriya, Phys. Rev. **120**, 91 (1960).

[25] K. Yosida, *Theory of Magnetism* (Springer-Verlag, Berlin, 1996).

[26] The ellipticity was estimated numerically by minimizing the total energy of the full model as a function of the

spin angles ϕ_i. The model was defined on one-dimensional chains of different lengths L with periodic boundary conditions and L ranging between 7 and 54, while the averaged spin components along the hard and easy axes were evaluated as $\overline{S^{h(e)}} = (1/L) \sum_{i=1}^{L} |S_i^{h(e)}|$, where $S_i^h = \cos \phi_i$ and $S_i^e = \sin \phi_i$.

[27] L. Chaix, R. Ballou, A. Cano, S. Petit, S. de Brion, J. Ollivier, L.-P. Regnault, E. Ressouche, E. Constable, C. V. Colin *et al.*, Phys. Rev. B **93**, 214419 (2016).

[28] I. S. Lyubutin, S. S. Starchikov, A. G. Gavriliuk, I. A. Troyan, Y. A. Nikiforova, A. G. Ivanova, A. I. Chumakov, and R. Rüffer, Appl. Phys. Lett. **112**, 242405 (2018).

[29] L. J. Bannenberg, R. Sadykov, R. M. Dalgliesh, C. Goodway, D. L. Schlagel, T. A. Lograsso, P. Falus, E. Lelièvre-Berna, A. O. Leonov, and C. Pappas, Phys. Rev. B **100**, 054447 (2019).

[30] See, https://www.crystran.co.uk.

[31] Note that the definition used in optics is just the other way around: The handedness of a material's optical activity is defined by the sense of rotation of the polarization plane when viewed from the detector towards the source. In this work we define the handedness as the sense of the structural chirality and as the sense of rotation of the polarization plane when viewed from the source towards the detector, i.e., a left-handed quartz sample corresponds to space group $P3_221$.